

Evidence of the stability of $\text{Mo}_2\text{TiAlC}_2$ from first principles calculations and its thermodynamical and optical properties

Gao Qing-He^{a,b}, Xu Zhi-Jun^c, Tang Ling^c, Zuo Xianjun^c, Jia Guozhu^d, Du An^{a*},
Linghu Rong-Feng^{e†}, Guo Yun-Dong^{ff}, Yang Ze-Jin^{c,g§}

^a(College of Science, Northeastern University, Shenyang, 110004, China)

^b(Information Engineering College, Liaoning University of Traditional Chinese Medicine, Shenyang 110847, China)

^c(School of Science, Zhejiang University of Technology, Hangzhou, 310023, China)

^d(College of Physics and Electronics Engineering, Sichuan Normal University, Chengdu 610068, China)

^e(School of Physics and Electronics Sciences, Guizhou Education University, Guiyang, 550018, China)

^f(College of Engineering and Technology, Neijiang Normal University, Neijiang, 641112, China)

^g(National Lab of Superhard Materials, Jilin University, Changchun 130012, China)

*gqhsu@163.com

†linghu@gznu.edu.cn

‡g308yd@126.com

§zejinyang@zjut.edu.cn

Abstract:

The elastic, thermodynamic, and optical properties of $\text{Mo}_2\text{TiAlC}_2$ are investigated by first-principles calculations. Our results indicate that the a axis is stiffer than c axis within 0~100 GPa. Elastic constants calculations predict the large stability range of $\text{Mo}_2\text{TiAlC}_2$ under pressure. Several important thermodynamic properties are discussed detailedly, including the Debye temperature, thermal expansion coefficient, and heat capacity *etc.* The bonding properties are studied from the elastic quantities and electronic properties. The electronic properties are investigated, including the energy band structure, density of states, and so on. The evidence of the instability of Mo_3AlC_2 and stability of $\text{Mo}_2\text{TiAlC}_2$ are successfully obtained.

Keywords: First principles; electronic properties; MAX phases;

1. Introduction

The $M_{n+1}AX_n$ ($n = 1, 2, 3$, etc) phases are a family of hexagonal compound, where M is a transition metal, A is an A-group element, and X is usually C or N. Since after Nowotny et al. synthesized a large number of MAX phases with $n=1$, which were called Hagg phases (denoted as "H-phases") [1], many experimental and theoretical studies devoted to MAX phases and their solid solutions[2]. Studies shown that MAX phases combine some of the best properties of metals and ceramics[3]. This considerably rare property combination arises from the more metallic M–A, more covalent M–X bonds and the presence of mobile basal plane dislocations.

Pressure can rapidly decrease the atomic distance and thus induces the novel structural transition, non-metals becoming metals and even superconductors[4]. Under high pressure, the light alkali elements Li[5] and Na[6] experience unusual metal-to-semiconductor transition. Usually, some end members of MAX phases become thermodynamically stable by forming quaternary compounds despite that one or both of the end members is thermodynamically unstable, such as $(Cr_{2/3}Ti_{1/3})_3AlC_2$ [7], $(Ti_{0.5}Nb_{0.5})_5AlC_4$ [8], $(Cr_{2/3}Ti_{1/3})_3AlC_2$ [9] and $(Cr_{3/8}Ti_{5/8})_4AlC_3$ [9], $(Ti_{1-x}Nb_x)_2AlC$ ($x = 0, 0.25, 0.5, 0.75, 1.0$)[10]. Phase stability of $(Cr_{1-x}, M_x)_2(Al_{1-y}, A_y)(C_{1-z}, X_z)$ ($M = Ti, Hf, Zr$; $A = Si, X=B$, prototype Cr_2AlC) was studied using *ab initio* calculations[11], in which only $(Cr_{1-x}, Ti_x)_2AlC$ compounds are stable, with x varying from 0 to 1 at an interval of 0.2.

Recently, Cr_2TiAlC_2 [7, 12], V_2CrAlC_2 [7, 12] and Mo_2TiAlC_2 phase[13] were synthesized. The geometry of Mo_2TiAlC_2 is isostructural with the other $M_{n+1}AX_n$

compound (such as Ti_3SiC_2) under the framework of same space group ($P6_3/mmc$)[13]. Experimental and theoretical characterizations of ordered MAX phases $\text{Mo}_2\text{TiAlC}_2$ and $\text{Mo}_2\text{Ti}_2\text{AlC}_3$ [14] are reported, in which many mechanical quantities and density of states (DOS) of $\text{Mo}_2\text{TiAlC}_2$ are studied. Many Ti-doping stabilized compounds are studied through formation enthalpy[15] calculations, and their DOS calculations, which demonstrate that Al/C atomic DOSs of $\text{Mo}_2\text{TiAlC}_2$ shifting towards lower-energy side contribute to the structural stability.

Many MAX compounds present very interesting behaviors under ambient conditions or high pressure, particularly for those Ti-related ones, such as the availability of $\text{Cr}_2\text{TiAlC}_2$ and $\text{Mo}_2\text{TiAlC}_2$ through doping one Ti atom from the unstable Mo-containing M_3AX_2 phases. Therefore, the new synthesized $\text{Mo}_2\text{TiAlC}_2$ might have interesting technological applications. Considering its special geometric structure, it is necessary to further study its thermodynamical and optical properties under pressure. We note that the Mo-containing MAX phases known to date are Mo_2GaC , $\text{Mo}_2\text{Ga}_2\text{C}$ and magnetic $(\text{Mo}_{0.5}\text{Mn}_{0.5})_2\text{GaC}$. Prior to the dopant of Ti atom, Ti atom stabilized Mo_2GaC presents unexpectedly *c*-axis ultraincompressibilities above about 15 GPa[16] as well as the hardest *c*-axis and softest *a*-axis and lowest transition pressure of $\text{Mo}_2\text{Ga}_2\text{C}$ [17]. Moreover, the group member of Ti atom (such as Zr atom) formed Zr_2InC [18] also presents the similar *c*-axis ultraincompressibilities above about 70 GPa. These phenomena indicate that the Ti atom and its group members formed novel chemical bonds at certain conditions. Furthermore, in order to fabricate Mo-based MXenes (a new family of two-dimensional (2D) materials labeled

MXenes by selectively etching the Al from Al-containing MAX phases), further investigations on the crystal structure of $\text{Mo}_2\text{TiAlC}_2$ are important to confirm the order of atoms in M sites for MAX compounds and to lay the foundation of Mo-based MXenes.

The motivations are to study the elastic stability and electronic properties of $\text{Mo}_2\text{TiAlC}_2$ under high pressure and to search if it displays any unusual behavior under extreme conditions. First principles are reliable method in calculating the elastic and electronics properties for the condensed matters[4-6, 19-23].

2. Computational methods

The structural optimization are performed by the Vanderbilt-type[24] ultrasoft pseudopotential with a generalized gradient approximation[25] for the Perdew–Burke–Ernzerhof exchange-correlation function. A plane-wave with 350.0 eV energy cut-off was applied, and the $10 \times 10 \times 2$ Monkhorst-Pack mesh was used at k -point sampling[26, 27]. Pseudo atomic calculations was performed for Mo $4d^5 5s^1$, Ti $3s^2 3p^6 3d^2 4s^2$, Al $3s^2 3p^1$, C $2s^2 2p^2$. The self-consistent convergence of the energy is at 5.0×10^{-7} eV/atom. Since the spin-polarized option is considered during the calculations on Mo_2GaC [28] we therefore also used this option for $\text{Mo}_2\text{TiAlC}_2$ throughout. All the calculations are done by CASTEP[29, 30].

3. Results and discussion

3.1 Elastic properties

$\text{Mo}_2\text{TiAlC}_2$ belongs to $P6_3/mmc$ and there are 12 atoms in one unit cell, the individual coordinate is: $(2/3, 1/3, u)$ of Mo, $(0, 0, 0)$ of Ti, $(0, 0, 1/4)$ of Al, $(1/3, 2/3,$

v) of C. The stable geometry parameters are obtained using the usual optimization procedure of hexagonal cell: $a=b=3.0157 \text{ \AA}$, $c=18.6032 \text{ \AA}$, $u=0.1352$, $v=0.0677$, consistent with the experimental data[13], $a=b=2.997 \text{ \AA}$, $c=18.6608 \text{ \AA}$, $u=0.13336$, $v=0.0687$, as is also shown in Table 1. Note that the properties of Mo_3AlC_2 comprising of its alpha and beta phases are calculated for reference only because they are unsynthesizable experimentally at ambient conditions. All of these calculated results agree excellent with the other calculations[14] and experimental measurements[13], confirming the reliability of the present calculations. The atomic space arrangements are shown in Figure 1.

Usually, the shrinkage along the c axis with pressure is faster than that along the a axis. Our calculations observe that a axis is always stiffer than c axis within 0~100 GPa, but the difference is vary small, as is shown in Figure 2. The volumetric shrinkage is far faster than that of axial shrinkage.

Elastic constants determine the response of the crystal to applied forces. Our calculated elastic constants are listed in Table 1 and Figure 3, together with other calculations[14]. Previous calculations[31] on Cr_2GeC , $(\text{Cr}_{0.5}\text{V}_{0.5})_2\text{GeC}$, and V_2GeC failed to find the higher moduli of intermetallics in comparison with its two end members, which is different with the experimental measurement. However, the present $\text{Mo}_2\text{TiAlC}_2$ occurs abnormal phenomenon, that is, almost all of the mechanical quantities are larger than its end members. Therefore, all of the calculated elastic moduli of $\text{Mo}_2\text{TiAlC}_2$ should be confirmed by the experimental confirmation. According to the stability criteria[32], *i.e.*

$$C_{12} > 0, C_{33} > 0, (C_{11} - C_{12})/2 > 0, C_{44} > 0, \\ (C_{11} + C_{12})C_{33} - 2C_{13}^2 > 0 \quad (1)$$

It is found that Mo₂TiAlC₂ is mechanical stable up to about 100 GPa. The small c_{33} manifests that the c -axis direction is relatively soft, which is consistent with the axial compressibility. As can be seen from Figure 3, the current $c_{11} > c_{33}$ means that the atomic bonds along the [100] planes between nearest neighbors are slightly stronger than those along the [001] plane. Besides, the comparable c_{33}/c_{11} and c_{13}/c_{12} means that the atomic bonding along the c axis is similar with that of a axis. Meanwhile, the c_{12} is always nearly equal with that of c_{13} at any pressures, and c_{44} presents similar variation trend with that of shear modulus G . These variation trends imply that the Mo₂TiAlC₂ should be stable in a wide pressure range.

Anisotropy factor $A = c_{33}/c_{11}$, $A=1$, meaning isotropic crystal, while any value larger or smaller than 1 indicates an elastic anisotropy. Analysis from the calculated elastic constants it is easily seen that Mo₂TiAlC₂ could be approximately viewed as isotropic material in a wide pressure range. The measurement of the elastic anisotropy in shear is given by the quantity $A_1 = c_{44}/c_s = 2c_{44}/(c_{11} - c_{12})$, where c_s is the shear modulus corresponding to an elastic wave propagation in the [110] direction. When c_{44}/c_s is equal to unity, a crystal is perfectly isotropic. The present Mo₂TiAlC₂ also could be approximately considered as isotropic material at 0 GPa, whereas the degree of isotropy decreases with the increasing of pressure, corresponding to 1.23 of 0 GPa and 1.91 of 100 GPa, respectively. The present result agrees with the calculated anisotropic factor, with a value of 1.27 at 0 GPa[14]. Another shear anisotropy

quantity is $A_2=(c_{11}+c_{33}-2c_{13})/4c_{44}$, when $A_2=1$, a crystal is perfectly isotropic. The present variation range of A_2 in $\text{Mo}_2\text{TiAlC}_2$ is 0.82 of 0 GPa and 0.5 of 100 GPa, consisting well with the conclusions of A_1 .

For covalent and ionic materials, the relations between bulk (B) and shear (G) modulus are $G\approx 1.1B$ and $G\approx 0.6B$, respectively. For $\text{Mo}_2\text{TiAlC}_2$ the calculated ratio of G/B (using their respective average values of Voigt, Reuss and Hill estimations) are in the interval from 0.715 at 0 GPa to 0.403 at 100 GPa, indicating that the ionic bonding is more suitable for $\text{Mo}_2\text{TiAlC}_2$ at ambient conditions and the degree of ionicity increases with pressure. To evaluate material ductility or brittleness, Pugh *et al.* introduced the B/G ratio[33]: the material is brittle if the ratio is less than the critical value (1.75) or the material is ductile if the ratio G/B is below 0.57. Our calculated $\text{Mo}_2\text{TiAlC}_2$ are brittle ($G/B = 0.715$) at zero pressure, and the degree of brittleness decreases at high pressure. Moreover, the current B/C_{44} is 1.44, within the range of $\text{M}_{n+1}\text{AX}_n$ phases 1.2-1.7. Poisson's ratio is generally used to quantify the stability of the crystal against shear and provides more information about the characteristics of the bonding forces than elastic constant. The value of Poisson's ratio for covalent materials is small (0.1), whereas for ionic materials a typical value is 0.25, and for metallic materials, a typical value is 0.33. The present Poisson's ratio is 0.2667 of 0 GPa and 0.3423 of 100 GPa, consisting with previous data, with a value of 0.25[14]. The present results means that the $\text{Mo}_2\text{TiAlC}_2$ is ionic materials and a higher metallic and ionic (or weaker covalent) contribution in inter-atomic bonding should be assumed, and the metallic or ionic increases gradually with pressure.

3.2 Thermodynamical properties

The thermodynamic properties of $\text{Mo}_2\text{TiAlC}_2$ are studied by the quasi-harmonic Debye model, the calculation details[34] could be obtained elsewhere. Many MAX phases will decompose at temperature above 2000 K, such as the stability limit of Ti_3SiC_2 [35] is 2300 K. The order-disorder transition temperature of M_2TiAlC_2 (M=Cr, Mo, W) is about 1773 K[15], which is far larger than the other MAX phases, meaning the important role of Ti-doping. Therefore, we calculate all these properties to about 1500 K. The Debye temperature Θ is a fundamental parameter of a material. Our calculated Θ is 708.58 K at $T=0$ K and $P=0$ GPa. From Figure 4, we can obtain: (a) When the pressure keeps constant (0, 30, 60, 90 GPa), the Θ decreases linearly with temperature. Moreover, the Debye temperature increases with pressure increasing, and the increase magnitude descends with same pressure interval. In particular, the Θ decreases extremely slow with temperature at higher pressure. (b) When the temperature keeps constant (0, 300, 600, 1000, 1500 K), the Θ almost increases linearly with pressure. The Θ at 1500 K is slightly lower than that at 0 K and the discrepancy gradually disappears at higher pressure. These data demonstrates its strong pressure and weak temperature dependences. This similar variation trends could also be found in the Grüneisen parameter, as is shown in Figure 5.

The variation of the thermal expansion coefficient α with temperature and pressure of $\text{Mo}_2\text{TiAlC}_2$ is presented in Figure 6. In Figure 6 (a), as pressure increases, α decreases rapidly and the pressure dependence decreased. Moreover, the discrepancy at 1000 K and 1500 K is small and the high temperature response is

rapidly decreased. In Figure 6 (b), α increases rapidly at low temperature and the increasing trend becomes gentler. The effects of pressure on α are smaller at low temperature than that at high temperature. Generally, α responds sensitively at lower temperature (below 500 K) and pressure (below 50 GPa), and the lower the temperature/pressure is, the faster the α changes. It can be found that the α converges to a constant value at high temperature and pressure.

The isothermal (B_T) and adiabatic (B_S) bulk moduli exist small differences owing to the very small thermal expansion coefficient α and Grüneisen parameter γ , $B_S=B_T(1+\alpha\gamma T)$. In Figure 7, both B_T and B_S bulk moduli decrease monotonically with temperature at zero or high pressure, but B_T varies significantly larger than that of B_S . Similarly, both B_T and B_S increase with pressure at zero or high temperature. The current investigations confirmed that B_S is always larger than B_T over a large pressure and temperature range and both of them increase with pressure at zero temperature.

According to the Debye temperature, we could calculate the lattice entropy S at different pressures and temperatures, as is shown in Figure 8. Clearly, when the pressure keeps constant, the S increases monotonously with temperature. On the contrary, when the temperature keeps constant, the S decreases monotonously with pressure, indicating its strong pressure and temperature dependences.

In Figure 9, the heat capacity at constant pressure C_P and at constant volume C_V with temperature T and pressure P are calculated. The computational results indicate that C_V and C_P increase with increasing temperature, the specific heat obeys the Debye T^3 power-law behavior in the low temperature limit, and C_V approaches the classical

asymptotic limit of $C_V = 3nNk_B = 149.54 \text{ J/mol}\cdot\text{K}$ for quaternary $\text{Mo}_2\text{TiAlC}_2$ at the temperature above 800 K. These characteristics of heat capacity show the fact that the interactions between ions in the nanolaminates have great effect on heat capacities especially at low temperatures. Furthermore, there is a difference between C_P and C_V in the normal state for the phases due to the thermal expansion caused by anharmonicity effects. The difference between C_P and C_V is small at low temperature. At high temperature, the C_V approaches a constant value, C_P increases monotonously with temperature increasing. In Figure 9 (a), (b), the discrepancy between C_P and C_V is negligible until 100 GPa under lower temperature (such as below 600 K), but the discrepancy slightly increased at higher temperature, such as 1500 K. Figure 9 (c), (d) reveals the minor difference of C_P and C_V at high temperature under 0 GPa. Under high pressure, the temperature dependences of C_P and C_V could be ignored reasonably due to the weak thermodynamical properties. These thermodynamical quantities present similar variation trends with the other MAX phases[36-40].

3.3 Electronic properties

For understanding the chemical bonding of $\text{Mo}_2\text{TiAlC}_2$, we have calculated the band structure and density of states (DOS) at 0 GPa and compared them with the available computations[14, 15]. As is seen from Figure 10, together with the hypothetical Mo_3AlC_2 , the total DOS of $\text{Mo}_2\text{TiAlC}_2$ reveals its metallic feature. The values of $\text{Mo}_2\text{TiAlC}_2$ and Mo_3AlC_2 at Fermi level are 5.5 and 9.9 electrons/eV,

respectively. The high value of Mo_3AlC_2 (alpha phase) corresponds to the occurrence of phonon imaginary frequency, as is shown in Figure 11.

The partial states (s , p , d) of Mo atom in $\text{Mo}_2\text{TiAlC}_2$ present quite similar distributions with those of Mo atom located along the c axis in Mo_3AlC_2 , only the d states display small discrepancy in the vicinity of Fermi level, as is shown in Figure 10 (b), (c). Such small discrepancy is caused by the different chemical environments as the Mo atom still occupies the same positions in the two compounds, namely, only those Mo atoms sited in the ab plane are substituted, as is also shown in Figure 1. In Figure 10 (d), the partial states (s , p , d) of Mo atom locating at ab plane in Mo_3AlC_2 show evident difference with those of Mo atom locating along c axis in $\text{Mo}_2\text{TiAlC}_2$. These differences include the relative shifts of s and p states and a profile change of d state. In Figure 10 (b), (d), a relative shift of s and p states of Mo atom towards higher-energy side in $\text{Mo}_2\text{TiAlC}_2$ occurs in comparison with the correspondent states of Mo atom locating at ab plane in Mo_3AlC_2 . However, such variation is far smaller than that of Ti atom, as is shown in Figure 10 (d), (e). Moreover, the small shift between the different Mo atoms for their same positions along c axis could be ignored reasonably, as is shown in Figure 10 (b), (c). This small shift denotes that these states are irrelativity to the structural stabilization. Unexpectedly, the value of d state of Ti atom at Fermi level is about 0.23 electrons/eV, which is far smaller than that of Mo atom at the same occupations, with a value of 1.25 electrons/eV shown in Figure 10 (d) (e). Such significant decrease, which is far larger than previous observations[15], can effectively stabilize the bond strength. This substantial decrease was partially

attributed to the less d orbital electrons of Ti atom. The s and p states of C atoms present a global shift towards lower energy side in Mo_3AlC_2 in comparison with those of $\text{Mo}_2\text{TiAlC}_2$, playing secondary role in stabilizing the lattice of Mo_3AlC_2 . In fact, the global shift of s and p states of C atoms in $\text{Mo}_2\text{TiAlC}_2$ might cause more charge overlap with d states of Ti and Mo atoms and therefore form stronger covalent bond. However, as is shown in Figure 10 (f), the negligible shift of s and p states of Al atoms between $\text{Mo}_2\text{TiAlC}_2$ and Mo_3AlC_2 possibly relates to its special in-plane occupancies, whereas previous calculations[15] observed the lower energy sites of the bonding states between Mo d and Al p in $\text{Mo}_2\text{TiAlC}_2$. The Mo d , Ti d , Al p , and C p electrons co-contribute to the energy range of $-10\sim 0$ eV.

Energy band analysis observes that four (51-54) and eight (51-58) orbitals cross Fermi level in $\text{Mo}_2\text{TiAlC}_2$ and Mo_3AlC_2 , respectively, completely consistent with the fact of high DOS value of Mo_3AlC_2 at Fermi level, as is shown in Figure 12 (a) (b). The large shift (about 0.75 eV) of G point towards high-energy side in $\text{Mo}_2\text{TiAlC}_2$ will strongly repulse the electrons shift to low-energy zone, making more electrons of Ti d states accumulate to the Ti-C bonding orientation and the edge of rhombic ab plane, totally consistent with the analysis of DOS in Figure 10 (d), (e). Moreover, less d orbital electrons of Ti atom built simpler energy level distributions around Fermi level, which could reduce the number of anti-bonding state. In particular, such unusual energy shift of G point will lead to stronger Ti-C bond due to the local energetic discrepancy, as is also the case of the energy distribution feature of A point, both of which are far lower than those of H and K points in energy, as is shown in

Figure 12. The coordinates of the special points are $G (0, 0, 0)$, $A (0, 0, 0.5)$, $H (-0.333, 0.667, 0.5)$, $K (-0.333, 0.667, 0)$, $M (0, 0.5, 0)$, and $L (0, 0.5, 0.5)$, respectively. This phenomenon is consistent with the facts of the orbital analysis, as is shown in Figure 13 (a) (b). Orbitals 51-54 demonstrate that little Ti d states of $\text{Mo}_2\text{TiAlC}_2$ contribute to the bonding, totally different with the cases of Mo_3AlC_2 . For better understanding the electron charge transfer direction, we also calculate the electron density differences and electron localization functions for the two compounds, as is shown in Figure 14. It is found that the substitution of Mo by Ti atom has led to significant charge transfer between C, Ti, and Mo atoms and formed stronger bond in $\text{Mo}_2\text{TiAlC}_2$.

3.3 Optical properties

To clarify the structural related properties, we also calculate the optical properties for radiation energy up to 45 eV via the absorption, reflectivity, energy loss, refractivity, dielectric, and conductivity coefficients *etc* at 0 GPa. The linear optical properties in solids can be described by the complex frequency-dependent dielectric function $\varepsilon(\omega) = \varepsilon_1(\omega) + i\varepsilon_2(\omega)$.

The imaginary part $\varepsilon_2(\omega)$ of the frequency-dependent dielectric function is given by

$$\varepsilon_2(\omega) = \frac{e^2 \hbar}{\pi m^2 \omega^2} \sum_{v,c} \int_{BZ} |M_{vk}(k)|^2 \delta[\omega_{cv}(k) - \omega] d^3k. \quad (1)$$

The integral is performed over the first Brillouin zone, and the momentum dipole elements $M_{vk}(k) = \langle U_{cv} | e \cdot \nabla | U_{ck} \rangle$, where e is the potential vector defining the electric field, are matrix elements for direct transitions between valence-band $u_{vk}(r)$

and conduction band $u_{ck}(r)$ states, and the $h\omega_{cv}(r) = E_{ck} - E_{vk}$ is the corresponding transition energy.

The real part $\varepsilon_1(\omega)$ could be derived from the imaginary part using the Kramers-Kronig relations,

$$\varepsilon_1(\omega) = 1 + \frac{2}{\pi} p \int_0^\infty \frac{\omega' \varepsilon_2(\omega')}{\omega'^2 - \omega^2} d\omega', \quad (2)$$

where p denotes the Cauchy principal value of the integral. Using the knowledge of real and imaginary parts of the frequency-dependent dielectric function, we thus can calculate the other optical functions.

The current incident photon polarization directions are $(1, 0, 0)$ and $(0, 0, 1)$, named $E \perp c$ and $E // c$ in these figures, respectively. The optical properties can be conveniently divided into two spectral regions, the low-energy range of 0~15 eV and the high-energy range of 35~40 eV, respectively.

In Figure 15, the large reflectivity index at low-energy range illustrates the strong optical response, consisting with the sensitivities of other properties. The calculated linear absorption spectrum presents two prominent peaks and the absorption edge starts from about 0 eV, corresponding to the energy pseudogap. The absorption thresholds along the two polarization direction are nearly the same. The absorption region is quite wide, the absorption intensity is quite large, which would make it a potential candidate for photoelectron application. The complex refractive index is composed of the real n and the imaginary part k . In the high energy range, such as above about 35 eV, n almost becomes a constant and k also decrease to zero, which show the system is relatively weak in absorption of high frequency wave. The

dielectric function presents similar variation trends with those of refractive index, its giant real part is clearly seen. The peaks at about 1 eV correspond probably to the transition between the Al p and C s states or the Ti p and Mo d states, where the ambiguous origin is attributed mainly to their similar peak intervals. Both the real and imaginary parts present onefold positive value. The calculated real and imaginary parts of the conductivity index are also presented. Both the real and imaginary parts respond sensitively in the energy range of 0~15 eV and 35~40 eV, respectively. The peaks of energy loss function correspond to the trailing edges of the refractive index n . The reflectivity also corresponds well to the energy loss spectrum.

4. Conclusion

We have performed comprehensive elastic, thermodynamic, electronic, and optical properties investigations for $\text{Mo}_2\text{TiAlC}_2$. The elastic properties confirmed the structural stability of $\text{Mo}_2\text{TiAlC}_2$ within 0~100 GPa. The structural instability of Mo_3AlC_2 for its two different phases are confirmed by the elastic constants and phonon dispersion curve. Furthermore, calculations on the energy band, density of states (DOS), orbitals, charge loss and gain features demonstrate that the high-energy zone of ab plane or rhombic center will promote the formation of stronger Ti-C bond. The fact of eight and four energy levels crossing Fermi level in Mo_3AlC_2 and $\text{Mo}_2\text{TiAlC}_2$ reveals the role of Ti atom in stabilizing the lattice during its substitution. The DOS of Ti atom determined the most likely origin of the lattice stability owing to its less d orbital electrons and simpler energy level distributions, as well as its special occupancies in the lattice.

Acknowledgement

Projects supported by the Natural Science Foundation of China (Grant No: 11304279, 11364007), Natural Science Foundation of Zhejiang Province, China (Grant Nos: LY13A040004, LY16A040013), China Postdoctoral Science Foundation (Grant No. 2012M520666), Science and Technology Foundation from Ministry of Education of Liaoning Province (Grant No: L2015333), and the Science and Technology Foundation from Guizhou Province (Grant No: J [2013]2242).

Reference

- [1] V. H. Nowtony, *Prog. Solid State Chem.* 5 (1971) 27
- [2] Z. M. Sun, *Int. Mater. Rev.* 56 (2011) 143.
- [3] H. Y. Wu, X. K. Qian, H. P. Zhu, J. Lei, and X. D. He, *Comp. Mater. Sci.* 84 (2014) 103
- [4] G. Y. Gao, A. R. Oganov, P. F. Li, Z. W. Li, H. Wang, T. Cui, Y. M. Ma, A. Bergara, A. O. Lyakhov, T. Litaka, and G. T. Zou, *Proc. Natl. Acad. Sci. USA* 107 (2010) 1317
- [5] J. Lv, Y. C. Wang, L. Zhu, and Y. M. Ma, *Phys. Rev. Lett.* 106 (2011) 015503
- [6] B. Manoun, O. D. Leaffer, S. Gupta, E. N. Hoffman, S. K. Saxena, J. E. Spanier, and M. W. Barsoum, *Solid. State. Commun.* 149 (2009) 1978
- [7] Z. M. Liu, E. D. Wu, J. M. Wang, Y. H. Qian, H. M. Xiang, X. C. Li, Q. Q. Jin, G. G. Sun, X. P. Chen, J. Y. Wang, and M. S. Li, *Acta Materialia* 73 (2014) 186
- [8] L. Y. Zheng, J. M. Wang, X. P. Lu, F. Z. Li, J. Y. Wang, and Y. C. Zhou, *J. Am. Cer. Soc.* 93 (2010) 3068
- [9] Z. M. Liu, L. Y. Zheng, L. C. Sun, Y. H. Qian, J. Y. Wang, and M. S. Li, *J. Am. Cer. Soc.* 96 (2013) 1
- [10] S. H. Ma, Z. Y. Jiao, and X. F. Huang, *J. Alloys Comp.* 591 (2014) 110
- [11] L. Shang, D. Music, M. Baben, and J. M. Schneider, *J. Phys. D: Appl. Phys.* 47 (2014) 065308
- [12] E. Caspi, P. Chartier, F. Porcher, F. Damay, and T. Cabioch, *Mater. Res. Lett.* 3 (2015) 100
- [13] B. Anasori, J. Halim, J. Lu, C. A. Voigt, L. Hultman, and M. W. Barsoum, *Scripta Mater.* 101 (2015) 5
- [14] B. Anasori, M. Dahlqvist, J. Halim, E. J. Moon, J. Lu, B. C. Hosler, E. N. Caspi, S. J. May, L. Hultman, P. Eklund, J. Rosen, and M. W. Barsoum, *J. Appl. Phys.* 118 (2015) 094304
- [15] M. Dahlqvist and J. Rosen, *Phys. Chem. Chem. Phys.* 17 (2015) 31810
- [16] Q. H. Gao, Z. J. Xu, L. Tang, J. Li, A. Du, Y. D. Guo, and Z. J. Yang, *J. Appl. Phys.* 119 (2016) 015901
- [17] Z. J. Yang, Q. H. Gao, Y. D. Guo, Z. J. Xu, and L. Tang, *Mod. Phys. Lett. B* 30 (2016) 1650105
- [18] Z. J. Yang, L. Tang, A. M. Guo, X. L. Cheng, Z. H. Zhu, and X. D. Yang, *J. App. Phys.* 114 (2013) 083506
- [19] Z. Y. Jiao, S. H. Ma, and T. X. Wang, *Solid State Sciences* 39 (2015) 97-104
- [20] Q. Li, D. Zhou, W. T. Zheng, Y. M. Ma, and C. F. Chen, *Phys. Rev. Lett.* 115 (2015) 185502
- [21] Y. W. Li, Y. C. Wang, C. J. Pickard, R. J. Needs, Y. Wang, and Y. M. Ma, *Phys. Rev. Lett.* 114 (2015) 125501
- [22] M. Zhang, H. Y. Liu, Q. Li, B. Gao, Y. C. Wang, H. D. Li, C. F. Chen, and Y. M. Ma, *Phys. Rev. Lett.* 114 (2015) 015502
- [23] Q. Li, Y. M. Ma, A. R. Oganov, H. B. Wang, H. Wang, Y. Xu, T. Cui, H. K. Mao, and G. T. Zou, *Phys. Rev. Lett.* 102 (2009) 175506
- [24] D. Vanderbilt, *Phys. Rev. B* 41 (1990) 7892-7895
- [25] J. P. Perdew, K. Burke, and M. Ernzerhof, *Phys. Rev. Lett.* 77 (1996) 3865-3868
- [26] A. Bouhemadou, *Appl. Phys. A* 96 (2009) 959
- [27] H. J. Monkhorst and J. D. Pack, *Phys. Rev. B* 13 (1976) 5188
- [28] M. Khazaei, M. Arai, T. Sasaki, M. Estili, and Y. Sakka, *Sci. Technol. Adv. Mater.* 15 (2014) 014208
- [29] M. C. Payne, M. P. Teter, D. C. Allen, T. A. Arias, and J. D. Joannopoulos, *Rev. Mod. Phys.* 64 (1992) 1045-1097

- [30] V. Milman, B. Winkler, A. White, C. J. Packard, M. C. Payne, E. V. Akhmatkaya, and R. H. Nobes, *Int. J. Quantum. Chem.* 77 (2000) 895-910
- [31] Z. J. Yang, J. Li, R. F. Linghu, X. S. Song, X. L. Cheng, Z. H. Zhu, and X. D. Yang, *Eur. Phys. J. B* 86 (2013) 208
- [32] M. Born, *Proc. Cambridge Philos. Soc.* 36 (1940)
- [33] S. F. Pugh, *Philos. Mag.* 45 (1954)
- [34] M. A. Blanco, E. Francisco, and V. Luana, *Comp. Phys. Comm.* 158 (2004) 57
- [35] A. G. Feng, T. Orling, and Z. A. Munir, *J. Mater. Res.* 14 (1999) 925
- [36] Z. J. Yang, Q. Liu, J. Li, Z. Wang, A. M. Guo, R. F. Linghu, X. L. Cheng, and X. D. Yang, *Sci. China-Phys. Mech. Astron.* (2013) 916
- [37] Z. J. Yang, J. Li, R. F. Linghu, X. L. Cheng, and X. D. Yang, *J. Alloys Comp.* 551 (2013) 435
- [38] Z. J. Yang, R. F. Linghu, X. L. Cheng, and X. D. Yang, *Acta Phys. Sin.* 61 (2012) 046301
- [39] Z. J. Yang, Y. D. Guo, R. F. Linghu, X. L. Cheng, and X. D. Yang, *Chin. Phys. B* 21 (2012) 056301
- [40] Z. J. Yang, Y. D. Guo, R. F. Linghu, and X. D. Yang, *Chin. Phys. B* 21 (2012) 036301

Table 1. The structural parameters and mechanical properties of $\text{Mo}_2\text{TiAlC}_2$. Note that the Voigt, Reuss, and Hill estimations of shear modulus G and Lamé λ are different, but the other moduli including the bulk modulus B , Young's modulus E on its three axial components (x , y , z) are identical. The units of these mechanical quantities are GPa, the lattice parameters are Å, and the volume is Å³, respectively.

	C_{11}	c_{33}	c_{44}	c_{12}	c_{13}	B	G	Lamé	$E_{x=y}$	E_z	a	c	V
$\text{Mo}_2\text{TiAlC}_2$	384	371	150	140	130	216	133	127	312	306	2.9987	18.7588	146.09
Cal.[14]	386	367	150	143	140	221	132				3.0082	18.757	
Exp.[13] ^a											2.997	18.661	
											2.93	18.9	
Mo_3AlC_2 (alpha phase)	373	350	132	143	131	212	122	130	296	183	3.0616	18.6170	151.1276
Cal.[14]	354	352	110	143	149	216	106				3.0714	18.542	151.48
Mo_3AlC_2 (beta phase)	289	368	-200	89	86	163	-14 (Voigt) 279 (Reuss) 132 (Hill)	173 (Voigt) -23 (Reuss) 74 (Hill)	251	329	3.089	19.8849	164.3323

^a: the lattice parameters are measured from two different methods, the values of 2.997 and 18.757 are obtained from the X-ray diffraction patterns, and the values of 2.93 and 18.9 are obtained from Selected area electron diffraction (SAED) characterization.

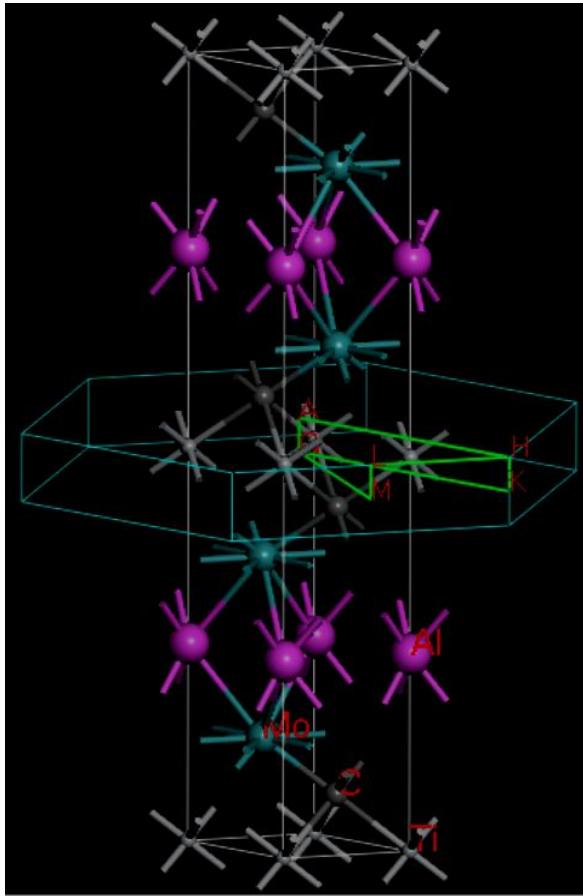


Figure 1. The lattice structure[11,13,14] of Mo₂TiAlC₂, together with the Brillouin zone, the horizontal lines are *ab* plane, and the vertical line is *c* direction. Mo₃AlC₂ can be obtained by replacing the Ti atoms in the *ab* plane by Mo atoms.

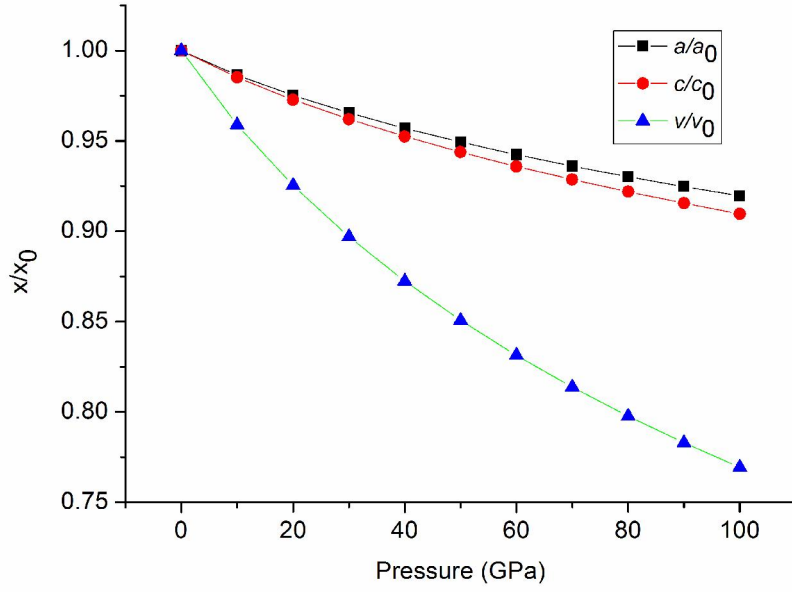


Figure 2. (Color online only). Axial compressibilities of a , c , and volumetric shrinkage of $\text{Mo}_2\text{TiAlC}_2$, where X represents a , c , and v at any pressures, X_0 represents a , c , and v at zero pressure.

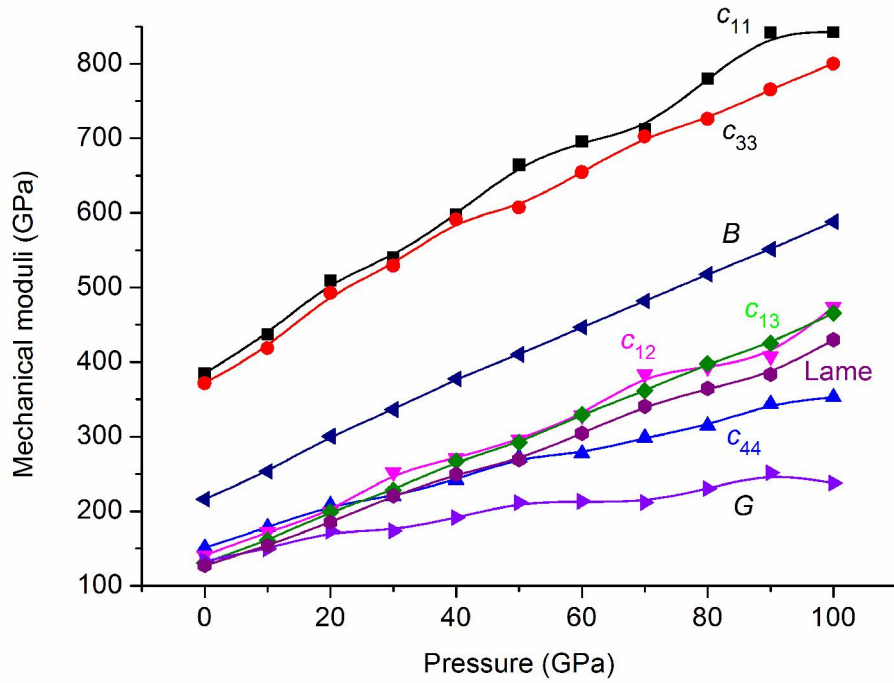


Figure 3. The elastic constants and mechanical moduli of $\text{Mo}_2\text{TiAlC}_2$ within 0~100 GPa at 0 K.

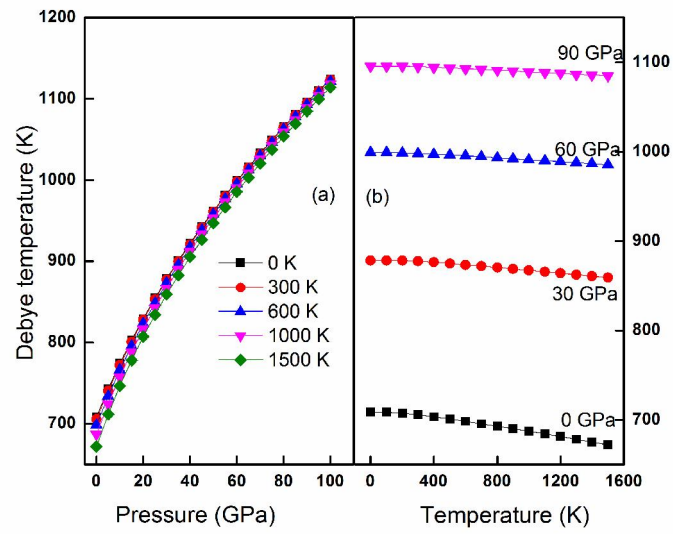


Figure 4. Debye temperature as a function of $\text{Mo}_2\text{TiAlC}_2$ under different temperatures and pressures.

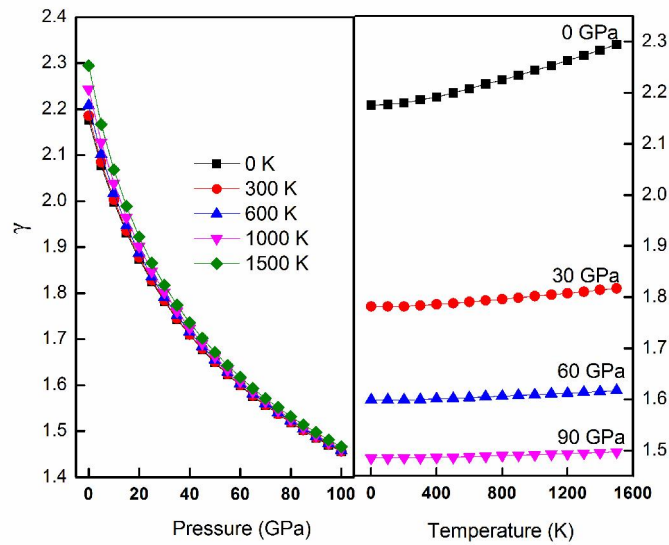


Figure 5. Grüneisen parameter as a function of $\text{Mo}_2\text{TiAlC}_2$ under different temperatures and pressures.

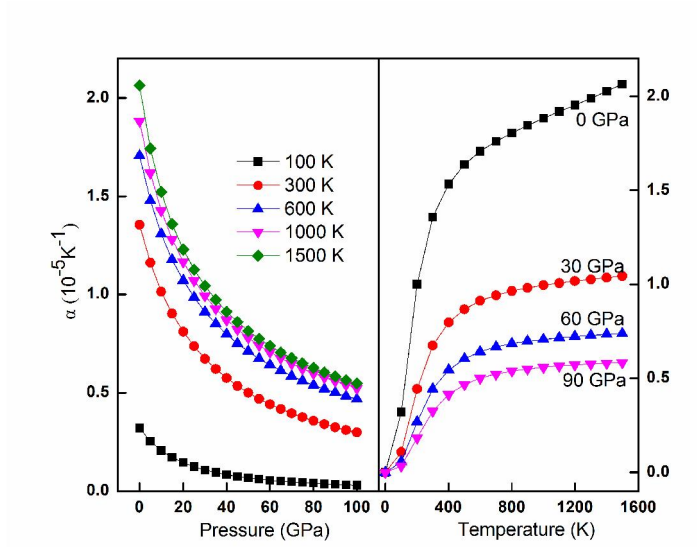


Figure 6. Thermal expansion coefficient of $\text{Mo}_2\text{TiAlC}_2$ as a function of temperature and pressure.

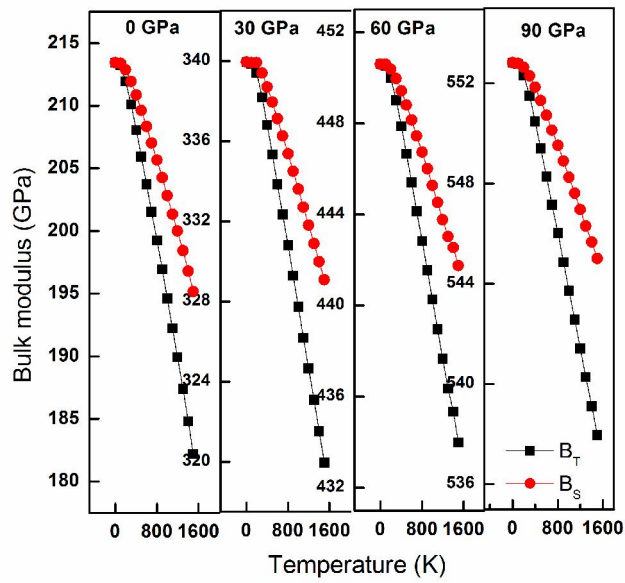


Figure 7. Isothermal (B_T) and adiabatic (B_S) bulk modulus of $\text{Mo}_2\text{TiAlC}_2$ under different temperatures and pressures.

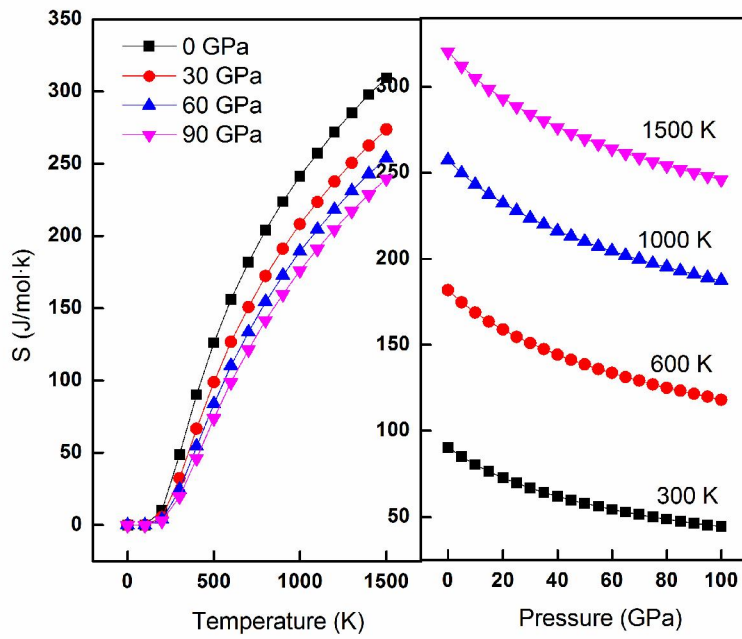


Figure 8. Lattice entropy as a function of $\text{Mo}_2\text{TiAlC}_2$ under different temperatures and pressures.

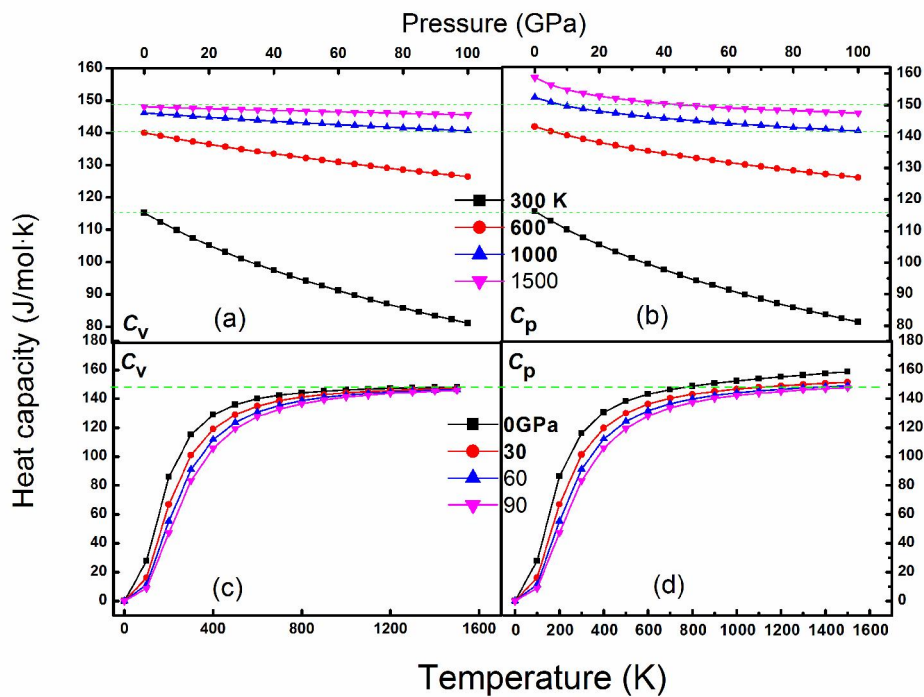


Figure 9. Heat capacity of $\text{Mo}_2\text{TiAlC}_2$ under different temperatures and pressures.

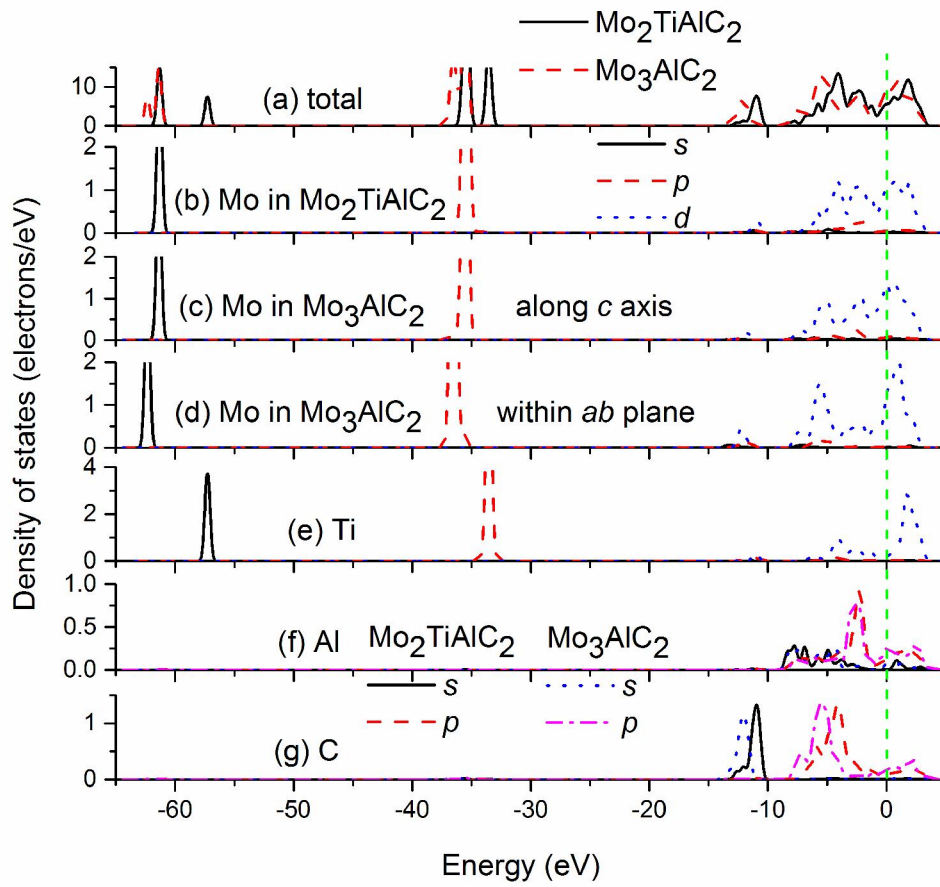


Figure 10. The density of states of $\text{Mo}_2\text{TiAlC}_2$ and the hypothetical Mo_3AlC_2 .

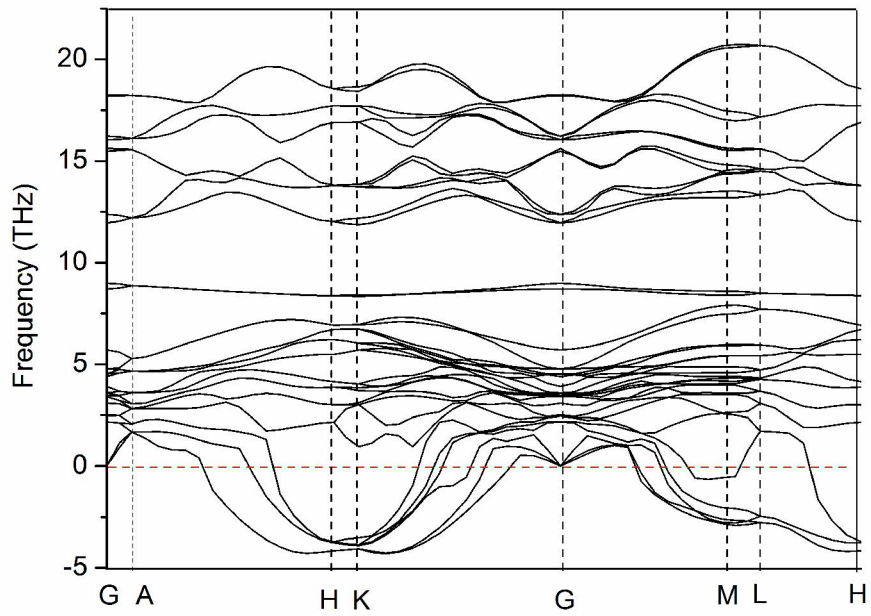


Figure 11. Phonon dispersion curve of Mo₃AlC₂ (alpha phase) at 0 GPa.

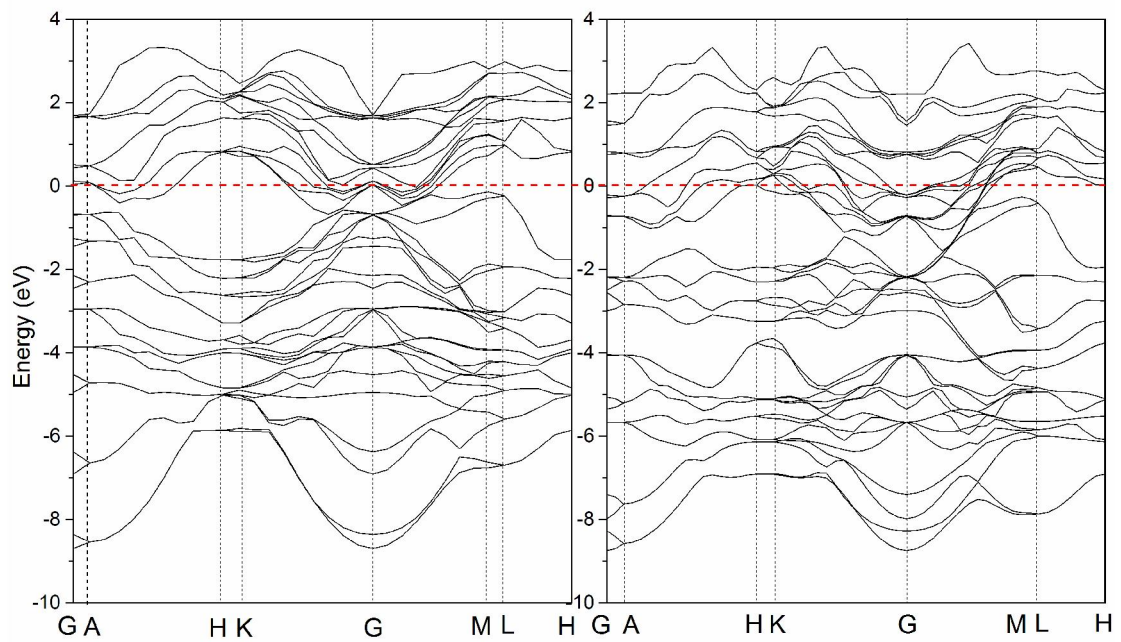


Figure 12 (a). Energy bands of Mo₂TiAlC₂ (left) and Mo₃AlC₂ near Fermi level.

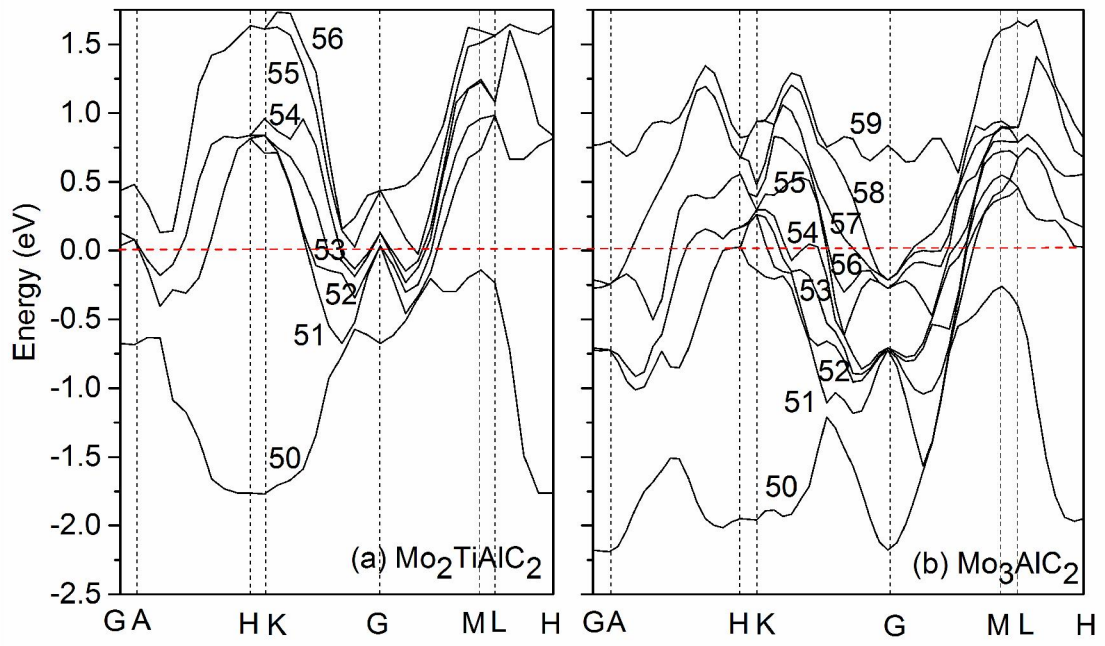


Figure 12 (b). Energy bands of $\text{Mo}_2\text{TiAlC}_2$ (left) and Mo_3AlC_2 that cross the Fermi level.

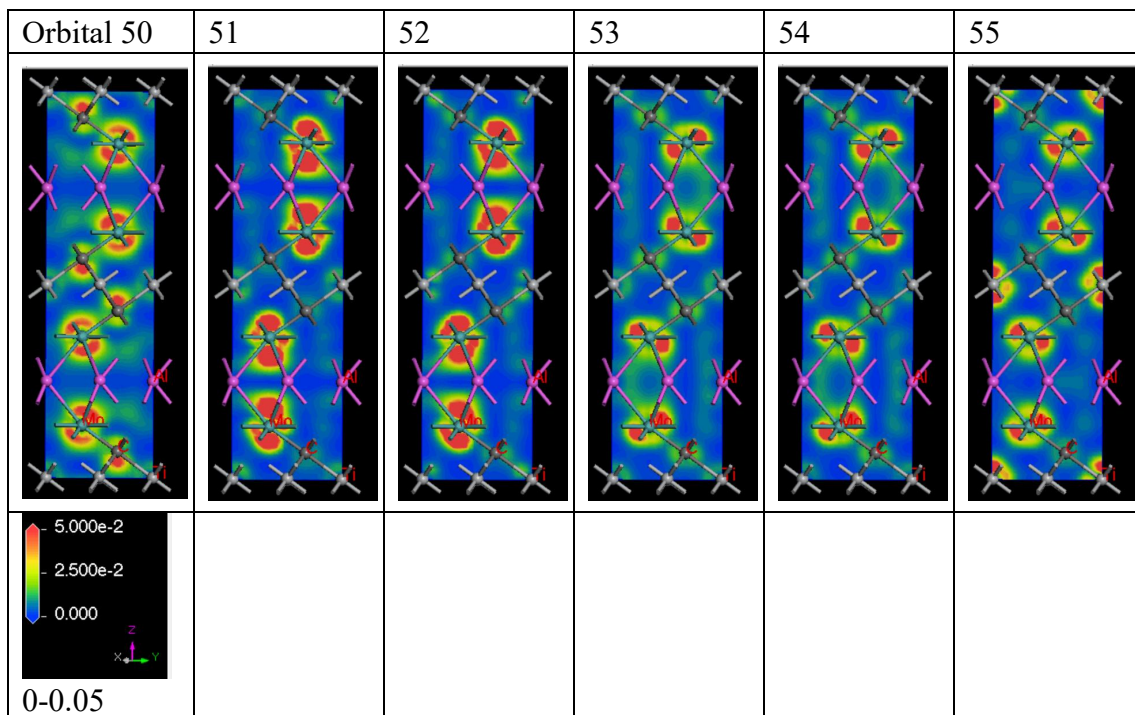
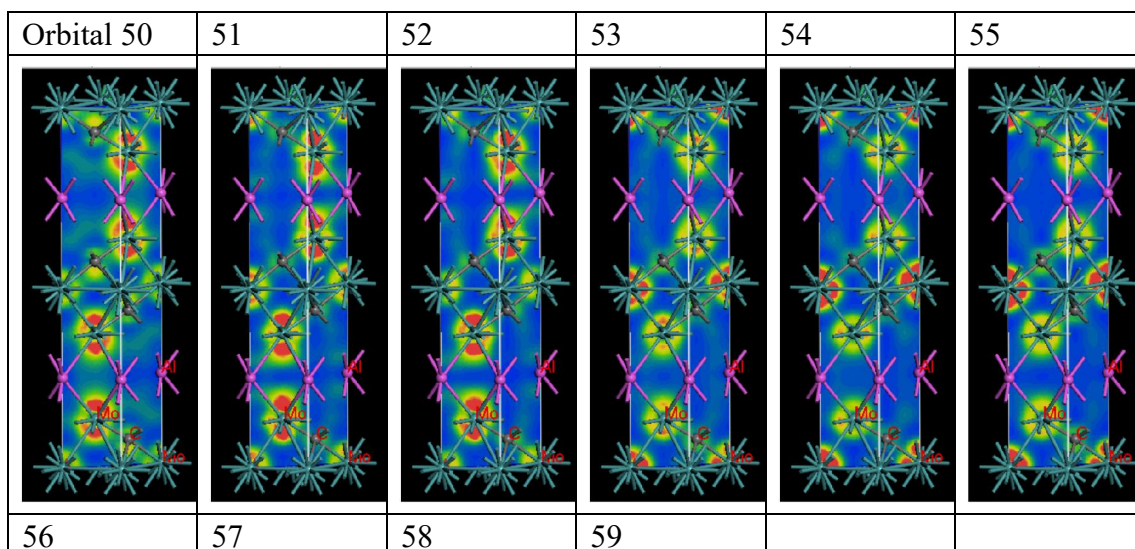


Figure 13 (a). Orbitals crossing Fermi level are shown in $\text{Mo}_2\text{TiAlC}_2$, together with their nearest neighbors 50 and 55. The color range is within 0~0.05 starts from blue, green, yellow, and red in turn. The horizontal axis x or y represents lattice a or b direction, vertical axis z means c direction.



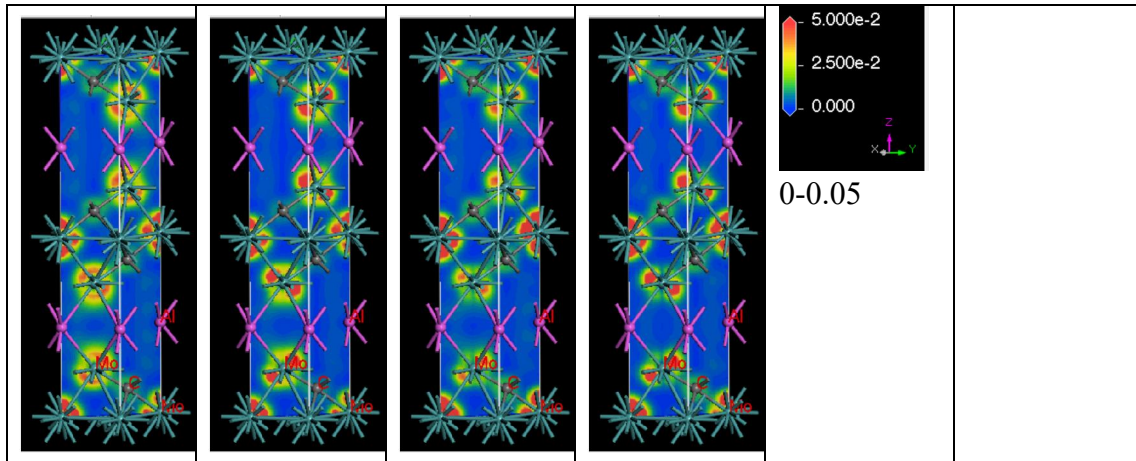


Figure 13 (b). Orbitals crossing Fermi level are shown in Mo_3AlC_2 , together with their nearest neighbors 50 and 59. The color range is same with that of Figure 13 (a).

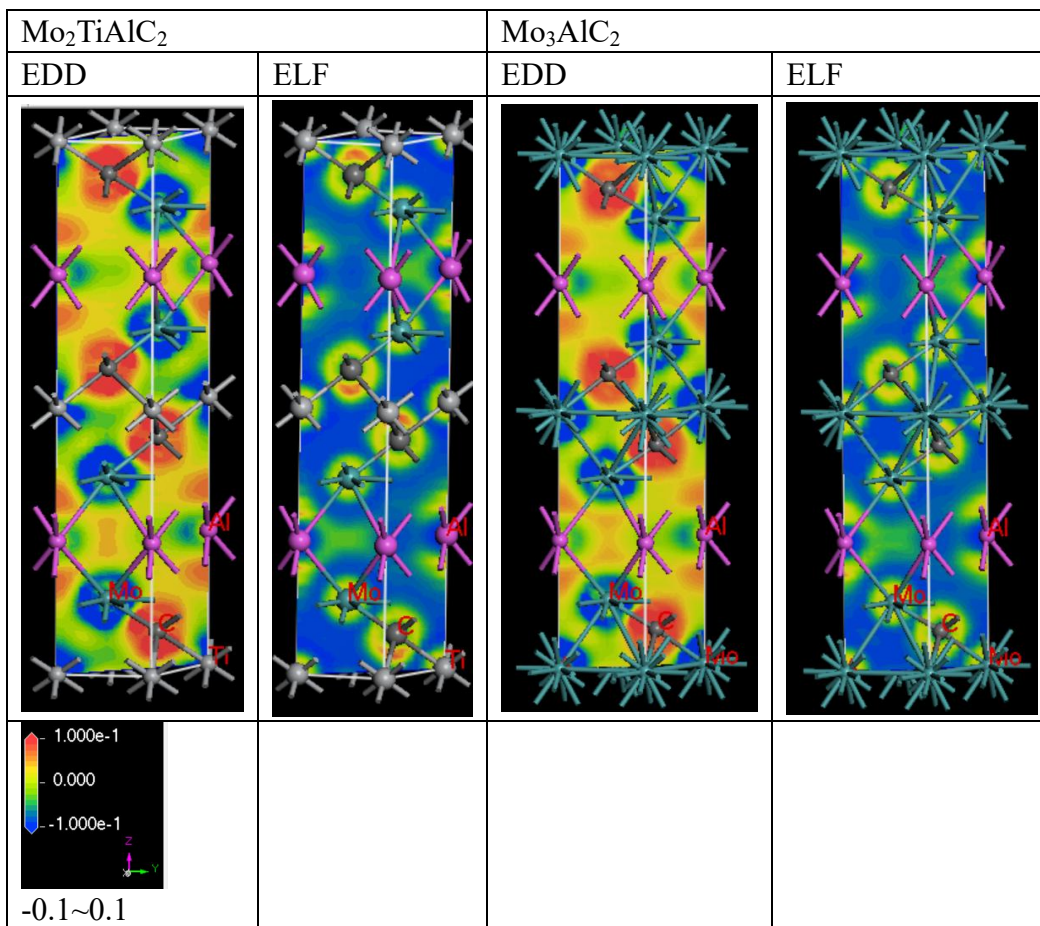


Figure 14. Electron density differences (EDD) and electron localization functions (ELF) of $\text{Mo}_2\text{TiAlC}_2$ and Mo_3AlC_2 . The color range is same with that of Figure 13 with the only exception of larger digital range $-0.1\sim 0.1$.

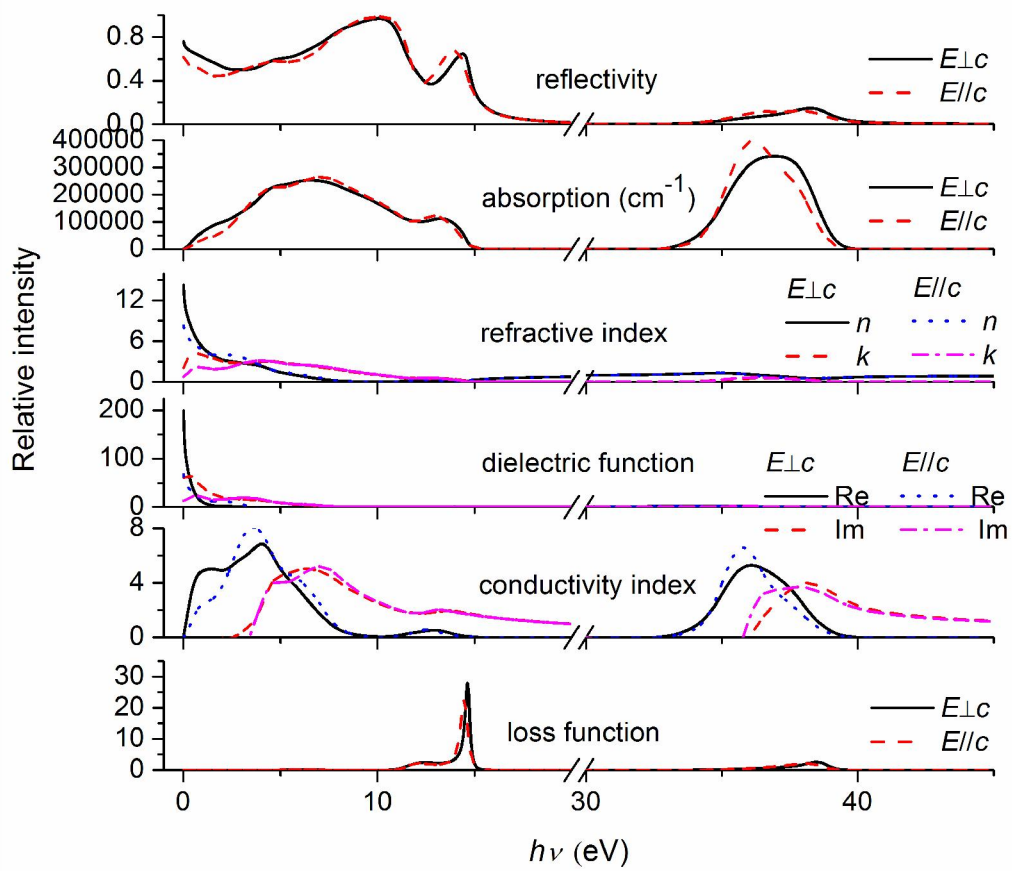


Figure 15. Optical properties of $\text{Mo}_2\text{TiAlC}_2$.